EARTH SCIENCES
RESEARCH JOURNAL
Earth Sci. Res. J. Vol. 29, No. 2 (June, 2025): 183 - 193

UNIVERSIDAD NACIONAL DE COLOMBIA

GEOLOGY

Introducing Quaternary magmatism of Gohar Kouh area with a focus on the lithological, geochemical and petrogenetic characteristics of the rocks (southeast of Iran)

Soudeh Sedighian
s.sedighian@velayat.ac.ir
Assistant Professor of Department of Geology, Velayat University, Iranshahr, Iran

ABSTRACT

The Gohar Kouh area, as a suspected tectonic region, consists of a collection of large folded structures, and is the core of a large arc called the Baloch arc, which is located in the southwest of the Sistan Suture Zone in the southeast of Iran. Young magmatism with olivine-basalt and basalt compositionally attributed to the Quaternary age has affected these units in the northern part. These lavas are composed of olivine, pyroxene, and plagioclase phenocrysts with low to moderate alteration, which are situated in a groundmass of plagioclase microlites and fine-grained pyroxenes and opaque minerals. Porphyry texture is the main texture of these rocks. Geochemical studies indicate that these rocks belong to the range of calc-alkaline basalts with moderate potassium and were formed as a result of the subduction of the oceanic crust of Oman under the Eurasian continental crust in the range of arc-related basalts in an active continental margin and a back-arc extensional environment. Investigation of trace element variations in these basalts proves the existence of lithospheric mantle origin. The presence of fluids resulting from subduction, involvement of sediments on the subducted crust, and crustal pollution are some of the reasons that have led to the enrichment of LILE elements compared to HFSE in the magma that created these rocks.

Keywords: Quaternary magmatism, Basalt, Continental arc, Back arc, Subduction, Oman oceanic crust.

Presentación del magmatismo cuaternario del área de Gohar Kouh con un enfoque en las características litológicas, geoquímicas y petrogenéticas de las rocas (sudeste de Irán)

RESUMEN

El área de Gohar Kouh, considerada una posible región tectónica, consiste de una colección de grandes estructuras sobrepuestas y es el centro de un arco grande llamado el arco de Baloch, el cual se localiza en el suroeste de la zona de sutura de Sistan, en el sureste de Irán. Magmatismo reciente compuesto de basaltos olivínicos y basaltos que se atribuyen a la edad cuaternaria han afectado estas unidades en la parte norte. Estas lavas están compuestas de olivino, piroxeno y fenocristales de plagiocasa con alteración entre baja y moderada, las cuales están situadas en una masa de tierra con microlitos de plagiocasa, piroxenos de grano fino y minerales opacos. La textura porfirítica es la principal de estas rocas. Estudios geoquímicos indican que estas rocas pertenecen al rango de basaltos calcoalcalinos con potasio moderado que se habrían formado como resultado de la subducción de la capa oceánica de Omán, bajo la capa terrestre continental Eurasiática y están en el rango de basaltos relacionados a un arco en un margen continental activo y en un ambiente extensional de arco de respaldo. La investigación de las variaciones de elementos traza en estos basaltos prueban la existencia del origen de un manto litosférico. La presencia de fluidos resultantes de la subducción, la presencia de sedimentos en la corteza subducida y la contaminación de la corteza son algunas de las razones determinantes para el enriquecimiento de elementos LILE en comparación con los elementos de alta intensidad de campo en el magma que creó estas rocas.

Palabras clave: magmatismo cuaternario; basalto; arco continental; arco de respaldo; subducción; corteza oceánica de Omán

Record
Manuscript received: 26/10/2024
Accepted for publication: 04/04/2025

How to cite this item:
Sedighian, S. (2025). Introducing Quaternary magmatism of Gohar Kouh area with a focus on the lithological, geochemical and petrogenetic characteristics of the rocks (southeast of Iran). *Earth Sciences Research Journa*l, 183-193 https://doi.org/10.15446/esrj.v29n2.117229

ISSN 1794-6190 e-ISSN 2339-3459
https://doi.org/10.15446/esrj.v29n2.117229

1. Introduction

The Sistan Suture Zone (SSZ) is an important connection in the middle part of the orogenic belt of the Himalayas and Zagros, the study of which is very important in understanding the tectonic conditions of Central Asia and the Middle East. This zone in eastern Iran separates the Lut continental block in the west from the Afghan block in the east with a north-northwest to south-southeast trend (Sengor, 1990; Mohammadi et al., 2016). The Sistan Ocean is a branch of the Tethys Ocean that was closed at the end of the Eocene (Mohammadi et al., 2016) and then affected by the strike-slip fault between the Central Iranian and Afghan blocks (Tirrul et al., 1983). Based on paleogeographic, structural, and petrographic studies, the eastward dip direction of the subducting plate has been identified (Camp and Griffis, 1982; Tirrul et al., 1983; Mohammadi et al., 2016). The Sistan Suture Zone consists of a deformed accretionary wedge and a flanking fore-arc basin. This range of three structural-sedimentary complexes separated by thrust faults (Camp and Griffis, 1982; Tirrul et al., 1983), includes the Ratuk Complex to the east, which is an older accretionary wedge, the Neh Complex to the west, which is a fold-thrust belt, and the Sefidabeh fore arc complex that covers unconformably both other complexes. Thrusting and strike-slip faulting have affected the basal stratigraphic on lap onto the underlying wedge turbidites (Tirrul et al., 1983; Mohammadi et al., 2016). SSZ has various types of igneous rocks, including ultramafic to felsic rocks found in ophiolitic complexes, intrusive rocks related to the granitoid belt of Garagheh-Saravan, extrusive and intrusive rocks related to Zahedan-Nehbandan magmatic belt and volcanic rocks related to the Taftan mountain activity (Camp and Griffis, 1982). The intrusive and extrusive masses in this area have been studied by many researchers (Tirrul et al., 1983; Mohammadi et al., 2016; Keshtgar et al., 2016; Sepidbar et al., 2018; Boomeri et al., 2019; Boomeri et al., 2020; Omidianfar et al., 2023). The study area is located in the eastern part of Iran, on the southeastern margin of the Lut block and the southwestern boundary of the SSZ, within the Neh Complex, and is associated with the Makran Subduction Zone (MSZ). The subduction of the Arabian Plate beneath the Eurasian Plate along the Makran plays a vital role in shaping the tectonic processes and magmatic activities in eastern Iran, influencing both the geological features and the formation of volcanic and plutonic rocks in the area. To date, no comprehensive studies have been conducted in this region. Therefore, the aim of this paper is to enhance our understanding of the conditions and environment associated with the formation of this area through fieldwork, petrographic, geochemical, and tectonic analyses. This complex tectonic interaction between the MSZ and the surrounding geological formations is crucial for understanding the region's overall magmatic evolution.

General geology

The Gohar Kouh volcanic masses are located in the southwestern part of Zahedan in the Sistan Suture zone (SSZ), southeastern Iran (Fig. 1-A). In general, Iran is a collection of several sedimentary-structural zones, and the SSZ is one of these zones, which is known in the east and southeast of Iran as a part of the remnants of the oceanic crust during the Cretaceous period, with a north-south trend and a length of over more than 700 km (Tirrul et al., 1983) (Fig. 1-A). This area is located between the Lut block on the west and the Afghan block on the east. The SSZ is divided into three sections: The Neh and Ratuk accretionary wedges and the Sefidabeh basin (Camp and Griffis, 1982; Rojhani et al., 2025). The Neh and Ratuk accretionary wedges are characterized by faulted and highly deformed ophiolitic mélanges, late Cretaceous to Eocene phyllites, and Paleogene marine clastic sedimentary rocks. On the other hand, the basin, in front of the Sefidabeh arc, contains small amounts of ophiolitic mélanges and a coherent and organized stratigraphy. According to Camp and Griffis (1982) and Tirrul et al. (1983), the non-ophiolitic igneous rocks in this zone differ from each other in terms of age, composition and origin, and they can be divided into four groups based on age: 1- Eocene calc-alkaline rocks attributed to the subduction of the Lut block beneath the Afghan block (Camp and Griffis, 1982); 2- I and S calc-alkaline Eocene-Lower Oligocene granitoids of Zahedan, which are related to the subduction and collision processes in the region (Camp and Griffis, 1982; Boomeri et al., 2005; Sadeghian et al., 2005; Sadeghian and Valizadeh, 2007; Rahnama-Rad et al., 2008; Ghasemi et al., 2010; Mohammadi et al., 2016); 3- Oligocene-Middle Miocene alkaline and calc-alkaline igneous rocks (Camp and Griffis, 1982), that are related to the activity of major faults in the eastern part of the region, which play a significant role in creating post-collision structural forms (Camp and Griffis, 1982; Walker and Jackson, 2004) and 4- Quaternary volcanic rocks similar to Taftan, which are attributed to the active subduction of Makran from the Arabian plate beneath the Makran accretionary wedge and the Sistan suture zone (Farhoudi and Karig, 1977; Boomeri et al., 2020; Delavari et al., 2022).

The magma that forms basaltic rocks is the primary magma, results from slight changes in the melting of peridotite rocks in mantle conditions; therefore, the survey of these rocks can provide valuable information regarding the origin, structure, and processing formation of their magma.

The Gohar Kouh Quaternary basaltic masses are scattered as several separate masses in the northern region of the Makran magmatic arc (Fig. 1-B). Based on the limited studies reported from these areas (Moinevaziri, 1985; Biabangard and Moradian, 2008; Pang et al., 2014) and the arrangement of these masses, a close relationship between the active subduction process in Makran and their magmatism can be recognized. However, there are still many ambiguities for their formation that need further investigation.

Regional Geology

Field observations on the volcanic rocks of the study area, which mainly have basaltic composition, show that these rocks are small and limited masses in size and extent with not very high topographies (Fig. 2-A and B). The Quaternary sediments that constitute a major part of the region, are covered by these volcanic rocks and show mostly dark color (dark brown to black) and purple in some areas (Fig. 2-C and D). Some parts of these masses, especially in the southwestern of the region, have a clear and distinct contact with metamorphosed carbonate rocks (dolomite and limestone) which, according to the Eftekharnezhad report (1992), are equivalent to the Jamal Formation with a probable Permian age (Fig. 2-C, D and E). The existence of metamorphosed enclaves within the volcanic rocks of the region at their contact confirms this possible age (Fig. 2-F). In this region, the dominant texture in the rock samples is aphanitic and vesicular texture, which shows a clear increase in the size of these vesicles in the basalt flows from the lower parts to the top of them.

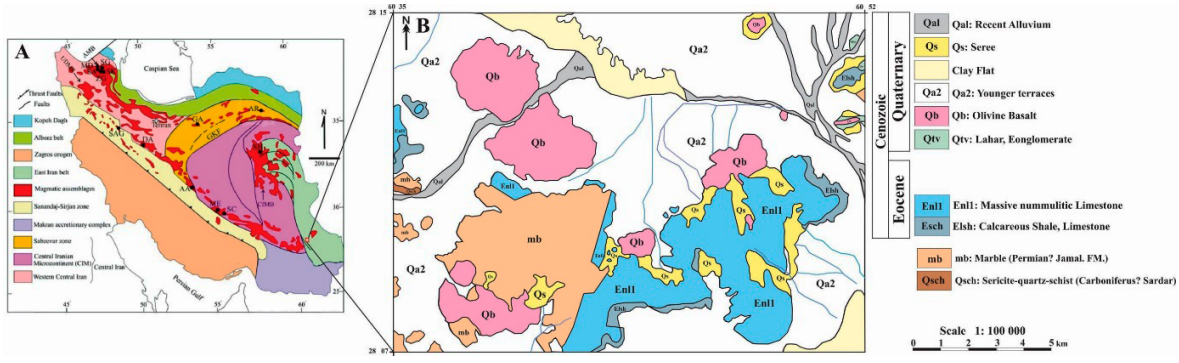

Figure 1. A: Major sedimentary-structural units of Iran (taken from Ashrafpour et al., 2012); B: The location of basaltic lavas of Gohar Kouh region in 1: 100 000 Dorjing sheet (Eftekharnezhad, 1992).

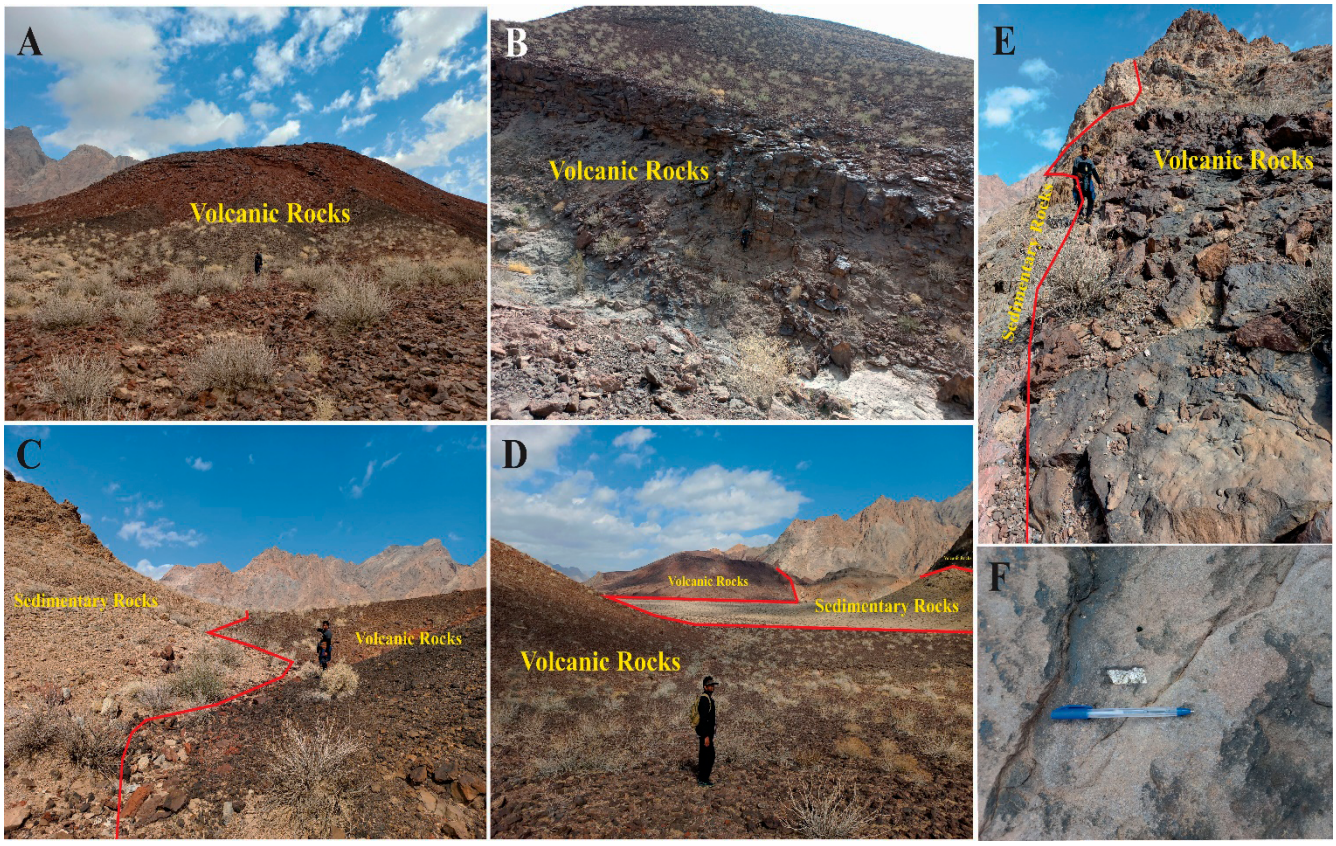

Figure 2. A and B**:** The presence of basaltic flows and lavas with relatively low topography in the area (View of the photos toward the northeast). C, D, and E: Clear contacts between lava flows and carbonate rocks, which have led to the alteration of these rocks in these areas (View of the photos toward the north (C) and east (D)). F: The existence of enclaves of metamorphosed carbonate rocks within the studied basaltic rocks.

2. Research method

In this research, after extensive field observations in the region, to conduct microscopic and geochemical studies, samples were collected from different parts of these igneous masses. Among these samples, 75 samples were selected for the preparation of microscopic thin sections and petrographic studies. For geochemical studies, 12 samples that were either unaltered or had minimal alteration were prepared and analyzed by using the Lithium Borate Fusion method for main elements and Inductively Coupled Plasma Mass Spectrometry for trace and rare earth elements in the laboratory of Zarazma Mineral Studies Company. Finally, various geological software such as Igpet and Minpet were used to process and interpret the results obtained from these analyses.

Petrography

Based on petrographic studies, the composition of the studied rock samples is mainly basalt, trachybasalt, and olivine basalt. The overall texture observed in these samples is a porphyritic texture with a fine-grained groundmass; however, trachytic, intergranular, glomeroporphyritic, and vesicular textures are the other textures that can be seen in the rock samples (Fig. 3). The degree of alteration in the rock samples is low to moderate. Olivine, pyroxene, and plagioclase are the most prominent crystals in these rocks. These crystals constitute about 70 to 75% of the volume of these rock groundmasses compared to the phenocryst crystals. Olivine phenocrysts (13-17%) are euhedral to anhedral (Fig. 3-A and F), with sizes ranging from 0.4 to 1.5 mm.

In some cases, these crystals are fractured and altered to iddingsite from the edges of the crystal (Fig. 3-B and F). This alteration indicates the existence of oxidizing conditions in the rock-forming environment during alteration, which occurs more frequently in olivines with lower forsterite and higher amounts of iron. The skeletal texture that can be observed in olivine crystals (Fig. 3-F) indicates a very high cooling rate and even a rapid solidification of the initial magma (Salas et al., 2021).

Pyroxenes, which are frequently observed as coarse crystals, are subhedral to anhedral and are less abundant than olivines. The size of these crystals is from 0.2 to 0.9 mm, and they are mostly located in the rock groundmass and the spaces between plagioclase microliths. The hourglass sector zoning can be seen in some pyroxenes (Fig. 3-A, C and E). The formation of this type of zoning indicates differences in crystal chemistry due to kinetic effects at the growth surfaces, whereby the elements are incorporated into the structure at different rates along different crystallographic surfaces, instead of changing the chemistry or conditions of the surrounding magma (Hollister and Guncarz, 1971). At least four controlling factors exist for creating hourglass sector zoning (Hollister and Gancarz, 1971): (1) the size and composition of ionic complexes added to the crystal during growth, (2) the rate of material addition, (3) the rate of equilibration of new material with groundmass on the growth surfaces, and (4) the rate of re-equilibration of surface layers with groundmass by ion exchange perpendicular to the crystal surfaces. Therefore, these crystals have grown so fast that they are ahead of their adjacent growing areas in terms of diffusion equilibrium (Schoneveld et al., 2020). The alteration degree of these crystals is not very high.

Plagioclase microliths, which constitute the majority of the rock groundmass (more than 43%), are in the range of labradorite exhibiting an average extinction angle of about 32 degrees. These crystals show a trachytic texture in most of the samples (Fig. 3-C). Iron oxides are visible as opaque minerals, comprising about 7% of these rocks (Fig. 3-D). The presence of magnetite and its inclusion by olivine and pyroxene crystals is a sign of the early crystallization of these minerals from a waterless magma; magnetites crystallize simultaneously with olivine in water-less magma. However, in hydrous magmas with low oxygen fugacity, this crystallization occurs in the later stages and after plagioclase crystallization (Hall, 1996). If there is an oxidizing condition in the basaltic magma crystallization, magnetite forms as a separate phase, which explains the higher presence of magnetite in olivine-bearing basalts compared to olivine-free ones (Gunnlaugsson et al., 2006).

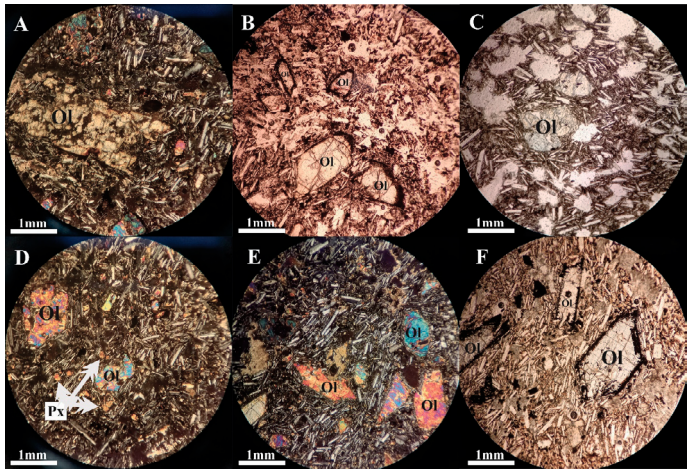

Figure 3. A and D: The presence of olivine phenocrysts within the groundmass of plagioclase microlites and fine-grained pyroxenes, porphyritic texture, in the rock samples of the study area; B and F: Evidence of Iddingsite around euhedral to subhedral olivine phenocrysts; C: Observation of flow and vesicular texture in the rock samples of the study area; E: Glomeroporphyritic texture in the Gohar Kouh basalts; F: Skeletal texture in the olivine crystals.

Geochemistry

In Table 1 and 2, the results of chemical analysis of rock samples from the Gohar Kouh volcanic masses are presented. In these samples, the LOI (Loss On Ignition) values range from 0.66 to 2.52% with an average of around 1.59%. These values indicate the relatively low alteration of these rocks, which can be confirmed by microscopic studies with only the presence of iddingsite margins around the olivine crystals and limited alteration. The range of SiO_2 values for these samples is from 46.96 to 51.13wt%. The Al_2O_3 values vary between 17 and 22.18wt% and CaO between 9.20 and 10.24wt%. The average Mg# (Mg#=(Mg/(Mg+Fe)) *100) for the basalts of the study area is about 61wt%, which can indicate their mantle origin (Christoph et al., 2017). The high amount of Al_2O_3 in these rocks may indicate the early crystallization of mafic minerals at relatively high pressure from their parent magma (Gust and Perfit, 1987; Yoder and Tilley, 1962), which led to an increase in the aluminum content in the residual melt and subsequently the crystallization of plagioclases at lower pressures.

Based on the Total Alkali-Silica (TAS) diagram (Le Bas et al., 1986), these rocks are in the range of basalts (Fig. 4). In the Le Maitre diagram (1989), the studied samples are located within the basalt range and medium-potassium calc-alkaline magmatic series (Fig. 5-A). Furthermore, to better distinguish the samples, the trace element diagrams were used. In the Hastie et al., (2007) diagram, which plots Th against Co, the studied samples also fall within the range of calc-alkaline series (Fig. 5-B).

Table 1. Geochemical results of rock samples from the study area for major elements by XRF method.

Sample	SiO_2	Al_2O_3	CaQ	Fe_2O_3	K_2O	MgO	MnQ	Na_2O	P_2O_5	SO_3	TiO2	SrO	LOI
TAN-1	50.57	17.12	9.73	7.26	0.71	7.91	0.13	3.65	0.13	*	0.73	*	2.07
TAN-2	50.22	17.35	9.54	7.32	0.64	8.16	0.13	3.63	0.12	0.42	0.74	0.07	1.67
TAN-4	50.21	17.48	9.68	7.07	0.57	7.68	0.13	3.78	0.11	0.96	0.73	0.08	1.52
TAN-5	50.49	17.5	9.55	7.37	0.65	7.89	0.13	3.68	0.12	0.43	0.75	*	1.44
TAN-6	48.3	17.94	10.21	8.02	0.75	7.12	0.13	3.67	0.14	0.58	0.94	0.07	2.13
TAN-7	50.23	18.15	9.46	8.04	0.9	7.04	0.13	3.6	0.13	*	0.95	*	1.36
TAN-8	50.15	18.22	9.2	8.44	0.99	7.36	0.14	3.57	0.17	*	1.04	0.07	0.66
TAN-9	46.96	17/00	10.24	7.71	0.91	6.9	0.13	3.35	0.16	3.1	0.95	0.09	2.52
TAN-10	49.7	0.19	9.82	7.92	0.82	7.07	0.14	3.63	0.19	0.13	0.94	*	1.74
TAN-12	51.13	17.31	9.6	7.21	0.71	7.62	0.13	3.75	0.14	*	0.75	*	1.65
TAN-13	50.81	17.71	9.61	7.37	0.67	8.21	0.13	3.77	0.1	0.08	0.73	0.07	0.73

Table 2. Geochemical results of rock samples from study area for minor and trace elements by ICP-MS method.

Sample	Ce	Cr	Cs	Eu	Gd	Hf	La	Li	Lu	Nb	Nd	Ni	P	Pb	Rb	Sb	Sc	Sm	Sr	Ta	Tb	Th	Ti	Tm	U	V	Y	Xb	Zr
TAN-1	24	254	0.9	0.89	3.34	3.2	12	7	0.2	14.4	14	121	722	30	21	0.8	18.8	2.2	468.6	0.1	0.5	2.2	3903	0.3	0.5	146	15.3	1.8	81
TAN-2	26	276	1	0.84	3.52	3.2	13	7	0.3	10	14.6	127	730	34	26	<0.5	20.3	2.5	518.4	<0.1	0.5	2.2	4056	0.3	0.7	152	16	1.83	87
TAN-4	23	232	0.9	0.91	3.54	3.5	13	5	0.3	8.5	14.6	123	741	43	23	<0.5	20.8	2.5	613.2	<0.1	0.5	2.2	4174	0.3	0.7	149	16.5	1.87	93
TAN-5	23	248	0.9	0.82	3.62	3.4	13	10	0.3	8.7	15	123	738	62	25	0.7	20	2.7	515	<0.1	0.5	2.3	4091	0.4	0.6	148	16.2	1.84	88
TAN-6	38	167	1.6	1.09	3.96	4.4	19	15	0.3	10	22.5	55	831	74	31	>0.01 %	24.9	3.6	566.3	<0.1	0.6	4.1	5342	0.4	0.7	170	19	2.18	73
TAN-7	35	177	1.1	1.19	4.08	3.3	19	17	0.3	7.4	23.4	58	832	68	33	10.8	26.3	3.5	497.7	<0.1	0.6	2.7	4943	0.4	0.7	160	18.8	2.18	73
TAN-8	47	187	1.6	1.26	4.29	4.7	23	8	0.3	9.7	25.3	51	928	56	36	0.7	28.2	4	612.8	<0.1	0.6	5.1	6066	0.4	1.1	189	21.1	2.45	141
TAN-9	44	193	1.5	1.24	4.1	4.3	21	12	0.3	11.7	24.1	48	844	33	42	1.9	24.2	3.6	700.7	0.2	0.6	4.4	5461	0.3	1	175	18.4	2.1	123
TAN- 10	38	156	1.1	1.16	4.12	4.1	20	10	0.3	8.5	22.8	54	829	28	29	<0.5	26.1	3.5	513.6	0.1	0.6	4	5413	0.4	0.7	148	20.7	2.28	122

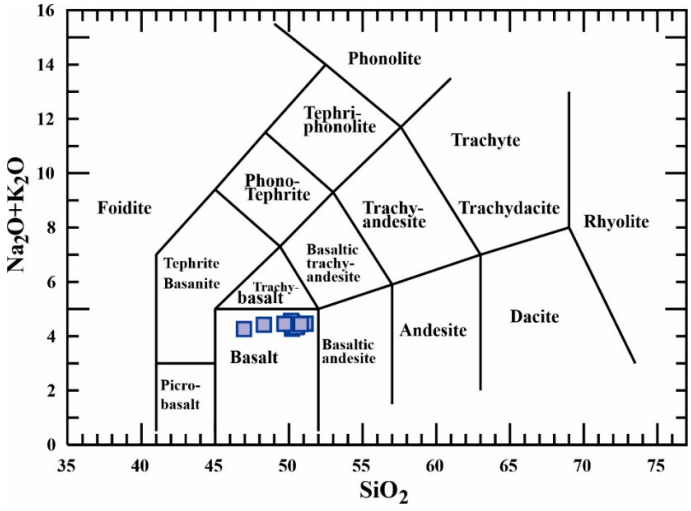

Figure 4. The plot of SiO_2 vs. Na_2O+K_2O (TAS) (Le Bas et al., 1986) where the studied samples are within basalt range.

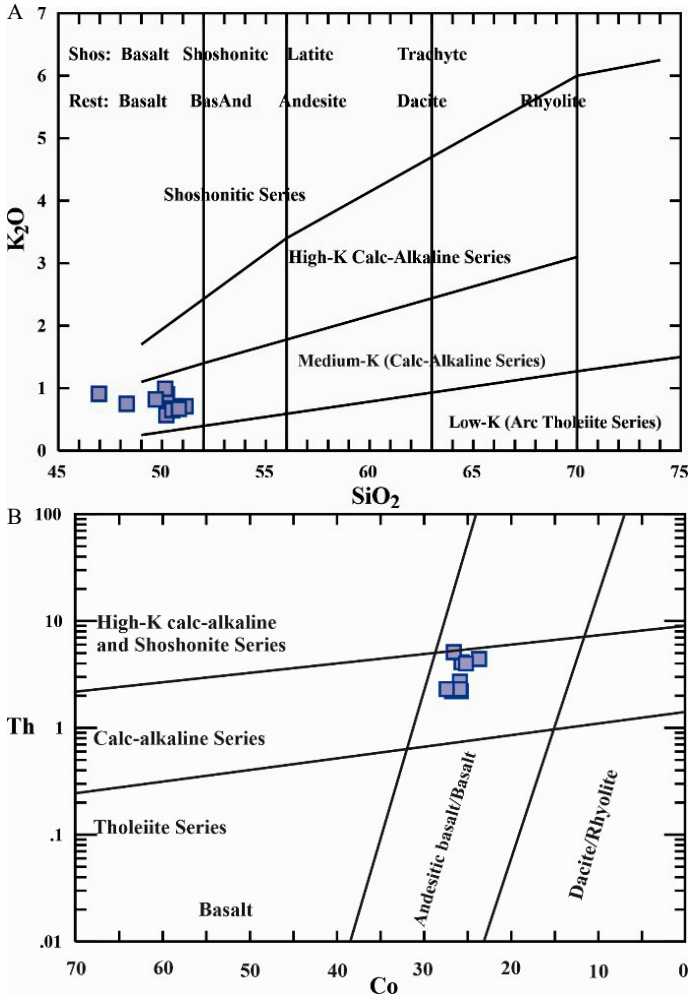

Figure 5. A: SiO_2 vs. K_2O diagram (Le Maitre, 1989) and B: Co vs. Th diagram (Hastie et al., 2007) to name and determine the magmatic series of the rock samples of the study area.

Based on the Middlemost diagram (1975), which distinguishes calc-alkaline or peraluminous basalts from tholeiitic basalts based on the Al_2O_3 content versus A.I.=((Na$_2$O+K$_2$O)/(SiO$_2$- 43)*(0.17)), these rock samples are within the range of peraluminous basalts (Fig. 6).

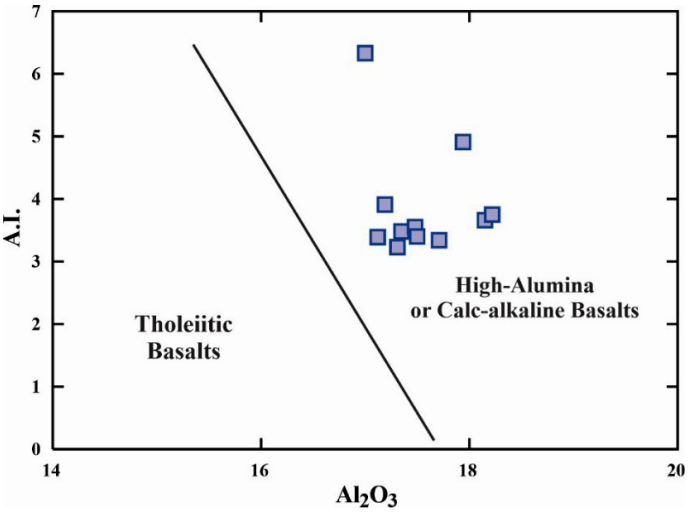

Figure 6. Al_2O_3 against [A.I.=((Na$_2$O+K$_2$O)/(SiO$_2$- 43)*(0.17))] (Middlemost, 1975), to determine the magmatic series and the potassium content of the study area samples.

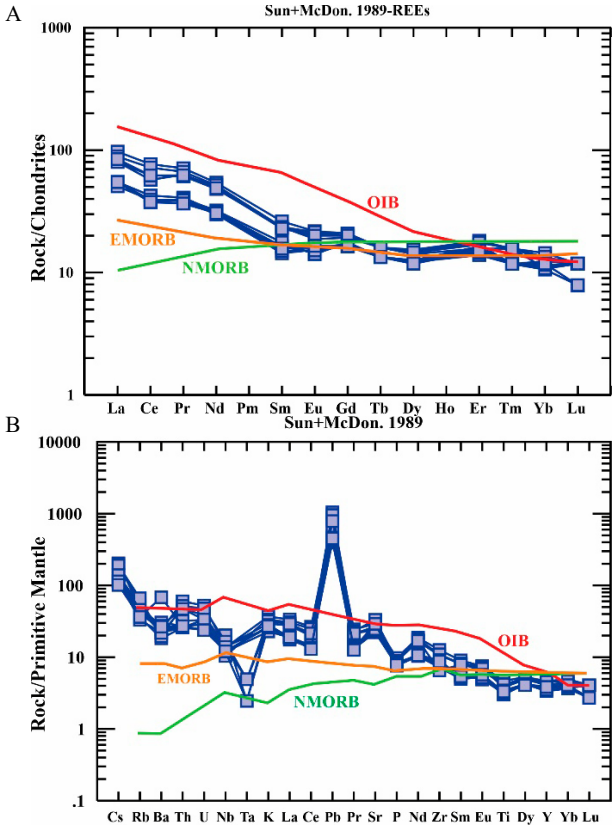

Figure 7. The variation patterns of elements in the basaltic rocks of the Gohar Kouh area in A: Chondrite-normalized REE diagram (Sun and McDonough, 1989); B: Primitive mantle-normalized spider diagram (Sun and McDonough, 1989). In these diagrams, the OIB, NMORB and EMORB patterns are included for comparison.

Tectonic setting implications

To determine the tectonic setting of basaltic magmas, there are several diagrams in which geochemical variations and different behavior of major, minor, and trace elements lead to the separation of different tectonic environments from each other. HFSE (High Field Strength Elements) and HREE (Heavy Rare Earth Elements) values are widely used to identify the tectonic environments of external rock samples (Pearce, 2008; Pearce and Peate, 1995). In the triangular diagram of Hf/3-Th-Nb/16 (Wood, 1980) (Fig. 8-A), all the studied samples fall within the range of arc-related basalts. In the V versus Ti/1000 diagram (Shervais, 1982), the behavior of melt and displacement of Ti, as well as the sensitivity of V to the oxidation state are combined. Shervais (1982) believes that with increasing in Ti/V ratio and increasing oxygen fugacity, the influence of subducting slab on basalt compositions increases. Therefore, the Ti/V ratio is very useful and effective for detecting the tectonic setting of basaltic rocks. All of the samples plotted clearly within the range of MORB and back-arc basin basalt (Fig. 8-B). Moreover, the La/Nb versus Y plot (Floyd et al., 1991) (Fig. 8-C), which is a suitable diagram for distinguishing between MORB and subduction-related eruptive environments, the studied samples also located within the range of back-arc basin basalts.

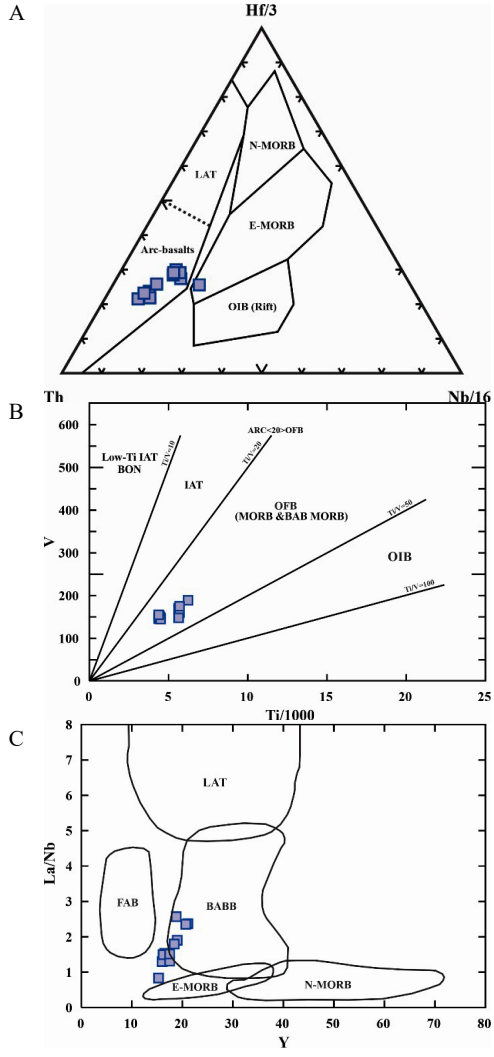

Figure 8. Tectono-magmatic discrimination diagrams of Gohar Kouh area. A: Hf/3-Th-Nb/16 diagram (Wood, 1980); B: V versus Ti/1000 diagram (Shervais, 1982); C: La/Nb versus Y diagram (Floyd et al., 1991).

The source and petrogenesis of magma

Investigating the geochemical characteristics of the Gohar Kouh basaltic rocks indicates that these volcanic rocks are arc-related basalts, specifically continental arc basalts (Fig. 9-A and B) that are produced in an active continental margin (Fig. 9-C) from an enriched source (Fig. 9-D).

In these basaltic samples, the depletion of HFSE compared to the adjacent LILE in the trace elements pattern normalized to the primitive mantle (Fig. 7-B) exhibits metasomatic activity related to the subduction process (Woodhead et al., 1993; Li et al., 2013; Zhou et al., 2006). The positive Sr anomaly and the absence of a distinct Eu anomaly show the small and insignificant influence of plagioclase in the evolution of these rocks (Floyd et al., 1991; Qian et al., 2016)). In the trace elements pattern of the samples normalized to the primitive mantle (Fig. 7-B), enrichment in LILE such as Cs, Rb, K, Pb, and Sr and depletion in HFSE such as Nb, Ta, P, and Ti is observed. The enrichment of Sr in these samples can be attributed to the absence of this element in common minerals (such as pyroxene) from the original magma and the substitution of Ca by Sr in plagioclase minerals. The negative Nb anomaly and the positive Pb and Sr anomalies in these rock samples indicate the contamination of magma with continental crust (Ozdemir, 2011) or the involvement of subduction components in the mantle source (Pang et al., 2013; Ozdemir, 2011) during rock formation in the region. The absence of negative Yb anomaly and the low ratio of Tb/Yb (0.27 on average) explained the absence of the residual garnet phase in the mantle source.

In addition, subduction-related provenance rocks are characterized by high La/Nb ratios (greater than 1.4) (Condie, 1999). Investigating the high La/Nb ratio (1.3-2.57) and the low Th/La ratio (0.15-0.23) in the rock samples exhibits a deformed lithospheric mantle source in the subduction zone for the volcanic rocks of Gohar Kouh. The low Nb and Ta values in the basaltic rocks may result from the existence of a pre-depleted mantle source or the preservation of Ti-rich minerals in the residual source area (Martin, 1999; Woodhead et al., 1993). The Nb/Th ratio less than 5 is indicative of a subduction zone where fluids released from the subducted slab are abundant, while the Nb/Th ratio greater than 7 is derived from melts in which fluids released from the subducted slab do not play a significant role in their formation. In the studied rock samples, this ratio is about 3.5, therefore, their relationship with the subduction zone and the influence of releasing fluids from the subducted slab are proven.

Moreover, investigating the relationships between Nb/La versus Zr/TiO_2 (Zhang et al., 2022) (Fig. 10-A) and La/Sm versus Th/Nb (Zhang et al., 2022) (Fig. 10-B) confirm the alignment of the basaltic samples with crustal contamination.

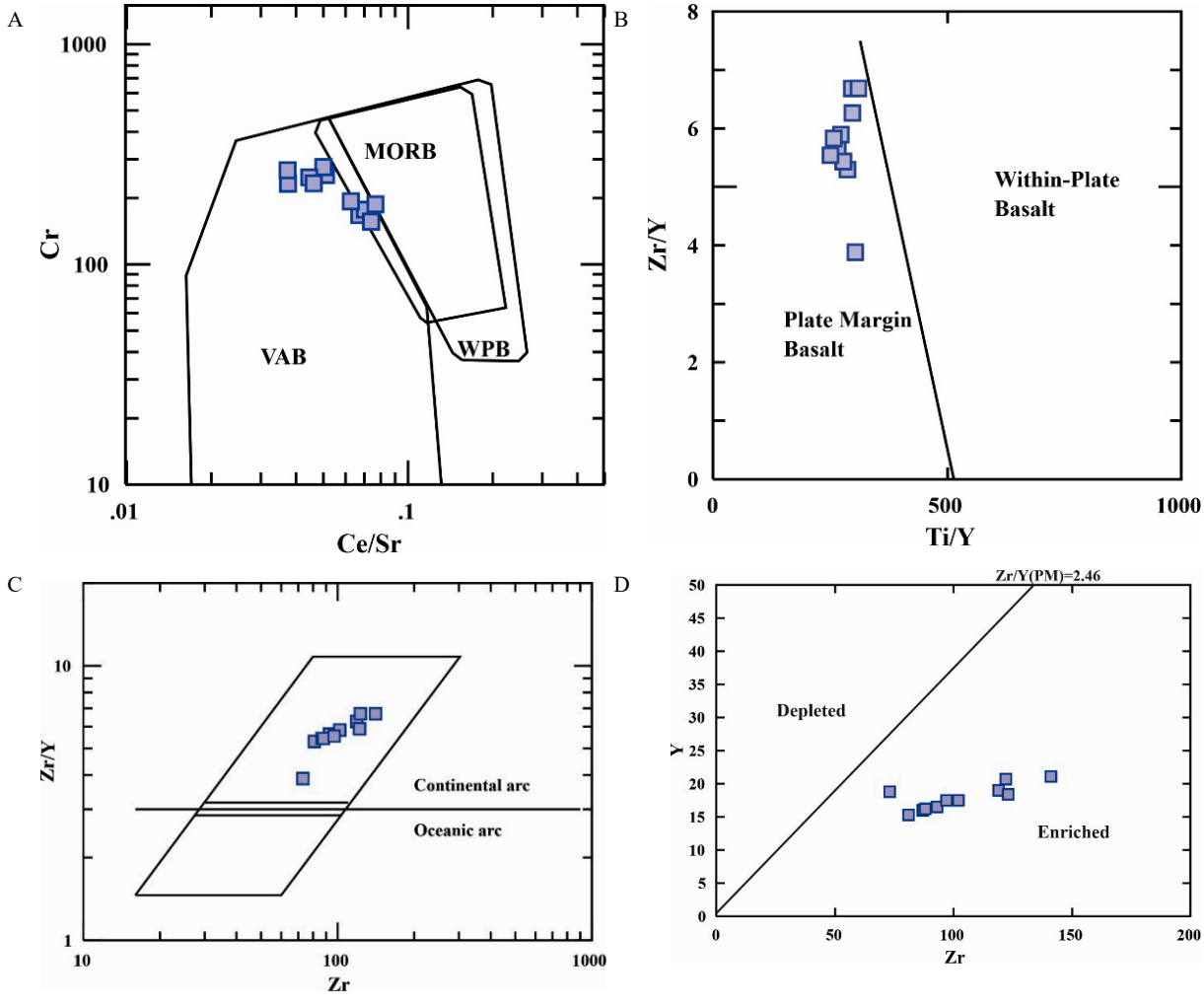

Figure 9. Discrimination diagrams of basaltic samples from Gohar Kouh area in A: Ce/Sr versus Cr diagram (Pearce, 1982); B: Ti/Y versus Zr/Y diagram (Pearce and Gale, 1977); C: Zr versus Zr/Y diagram (Pearce, 1983) and D: Zr versus Y diagram (Sun and McDonough, 1989). These diagrams are drawn based on the nature of the less mobile elements and their sensitivity to the source composition.

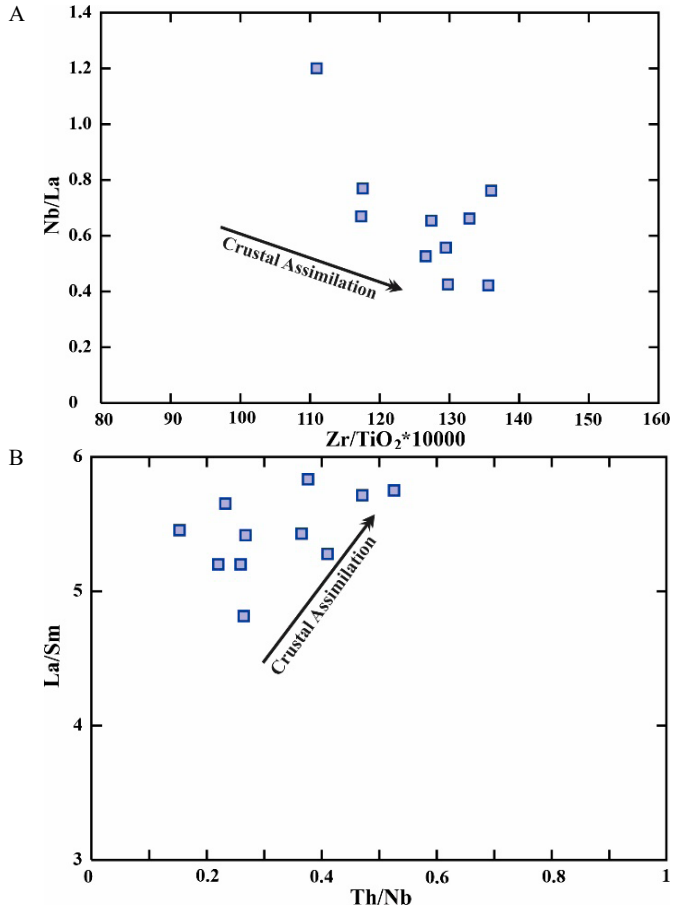

Figure 10. A: Nb/La versus Zr/TiO_2 diagram (Zhang et al., 2022); B: La/Sm versus Th/Nb diagram (Zhang et al., 2022), to investigate the crustal contamination process based on the chemical variations of the rock samples.

Also, the sediments overlying the subducted oceanic crust have similar trace element distribution patterns compared to the continental crust (Plank and Langmuir, 1998; Zhang et al., 2022), so that, the significant negative Nb, Ta, and Ti anomalies and the cycling of these materials at the source, cause the observed reduction of HFSE in the rock samples of the region (Fig. 7). The Th/U ratio can also be used to investigate crustal contamination. This ratio in the upper crust is about 3.8 (Rudnick and Gao, 2014) and in the studied rocks is about 4.3. So, it can be a sign of crustal contamination.

Based on the Th/Yb versus Nb/Yb plot (Pearce, 2014) (Fig. 11), the origin of the rock samples can be considered within the compositional range between OIB and E-MORB. In this diagram, all the studied samples are displaced from the mantle array, which indicates that they were influenced by subduction material with arc-like signatures (Faisala et al., 2020). The metasomatic processes in these conditions may involve aqueous fluids, primary melts from partial melting of the sediments, or basaltic subducted slab into the mantle wedge, which leads to decreasing the solidus temperature in the mantle, partial melting, and producing the magma (Harangi et al., 2007; Hoang et al., 2011). The Zr/Nb ratio in the studied samples (this ratio is less than 10 in OIB, about 10 in E-MORB, and around 40 in N-MORB (Pearce and Norry, 1979)) is about 10.74. So it can be concluded that these samples have closer characteristics to E-MORB. Therefore, it is suggested that, in addition to the enrichment created by releasing fluids, the mantle source of these basaltic rocks has been enriched with incompatible trace elements.

Basalts, especially those with MgO content above 6 wt%, which have undergone the least magmatic changes and transformations, are considered the most suitable rocks for modeling mantle melting (Niu, 2021). The Sm/Yb (1.2-1.72) against La/Sm (5.8-4.8) values for the basalts of the studied area show that these rocks located in a lower range than garnet lherzolite and close to the melting curve of spinel lherzolite with a low degree of partial melting (around 2 to 10%) (Aldanmaz et al., 2000) (Fig. 12-A). This is consistent with the normalized pattern of the studied rocks relative to chondrite (Fig. 7-A) and indicates that their parental magma formed at shallow depths and as a result of low degrees of partial melting. The Dy/Yb ratio of these samples (around 1.66) also confirms the origin in the range of spinel lherzolite. The La/Yb ratio in the rock samples of the region, which varies in the approximate range of 6.64 to 10, indicates the absence of garnet in the residual phase in the source area, and consequently, their parental magma must have been produced at depths of less than 40 km (Haschke et al. al., 2002; Faisal et al., 2020). A high Nb/La ratio (more than 1) exhibits an asthenospheric mantle source, while a lower ratio (approximately less than 0.5) indicates a lithospheric mantle source (Smith et al., 1999). This ratio is around 0.64 for the Gohar Kouh samples, which indicates the lithospheric mantle source (Fig. 12-B).

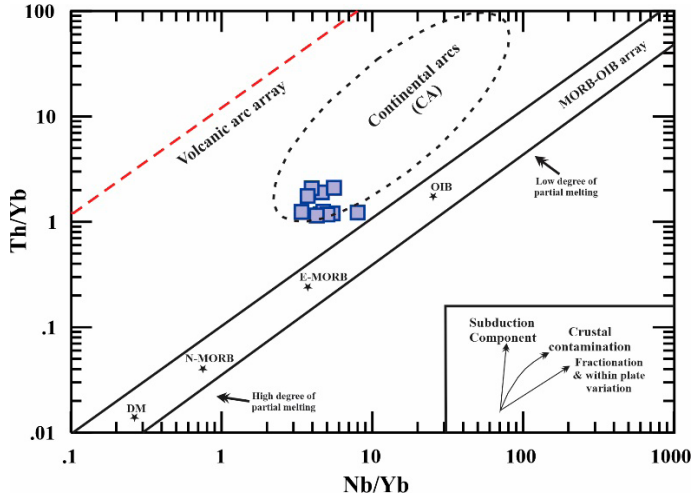

Figure 11. The position of the studied samples on Th/Yb versus Nb/Yb diagram (Pearce, 2014).

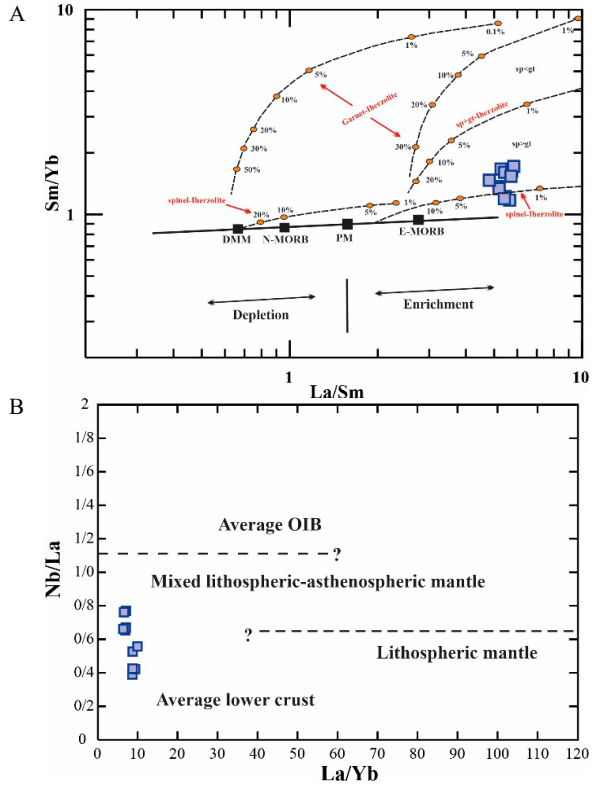

Figure 12. A: La/Sm versus Sm/Yb diagram (Aldanmaz et al., 2000); B: The variation of Nb/La against La/Yb (Aydin et al., 2008). The asthenospheric, lithospheric and their combined mantle field identified in this diagram.

Conclusion

The young calc-alkaline basaltic rocks of Gohar Kouh consist of basalt, trachybasalt, and olivine basalt. Olivine, pyroxene, and plagioclase are the most important minerals in these rocks. This region is located in the southeast of Iran and is part of the SSZ, which formed as a result of the subduction of the Oman oceanic crust beneath the Eurasian continental crust in an active continental margin and a back-arc extensional environment. These rocks are derived from partial melting products with a low degree (about 2 to 10%) within the spinel lherzolite range. Their source may be an enriched mantle with higher concentrations of LILE elements compared to HILE. The negative Nb anomaly, positive Pb and Sr anomalies, as well as the Th/U ratio around 3.4 in these samples, indicate magma contamination with the continental crust. Additionally, the Nb/Th ratio around 5.3 suggests a connection between these parental magmas and the subduction zone, with the influence of fluids released from the subducted slab.

Acknowledgments

The author sincerely appreciates Mr. Shamsoddin Damani Gol at the Department of Geology, Velayat University, Iran, for his valuable suggestions, extensive assistance in conducting this research.

References

Aldanmaz, E., Pearce, J., Thirlwall, M. & Mitchell, J. (2000). Petrogenetic evolution of late Cenozoic, post-collision volcanism in western Anatolia, Turkey. Journal of Volcanology and Geothermal Research, 102, 67-95. https://doi.org/10.1016/S0377-0273(00)00182-7.

Ashrafpour, E., Ansdell, K.M. & Alirezaei, S. (2012). Hydrothermal fluid evolution and ore genesis in the Arghash epithermal gold prospect, northeastern Iran. Journal of Asian Earth Sciences, 51, 30-44. https://doi.org/10.1016/j.jseaes.2012.01.020.

Aydin, F., Karsli, O. & Chen, B. (2008). Petrogenesis of the Neogene alkaline volcanics with implications for post -collisional lithospheric thinning of the Eastern Pontides, NE Turkey. Lithos, 104, 249-266. https://doi.org/10.1016/j.lithos.2007.12.010.

Biabangard, H. & Moradian, A. (2008). Geology and geochemical evaluation of Taftan Volcano, Sistan and Baluchestan Province, southeast of Iran. Chinese Journal of Geochemistry, 27, 356-369. https://doi.org/10.1007/s11631-008-0356-z.

Boomeri, M., Lashkaripour, G. & Gargich, M. (2005). F and Cl in biotites from Zahedan granitic rocks. Iranian Journal of Crystallography and Mineralogy, 13, 79-94. https://sid.ir/paper/3786/en.

Boomeri, M., Moradi, R. & Bagheri, S. (2020). Petrology and origin of the Lar igneous complex of the Sistan suture zone, Iran. Geologos, 26(1), 51-64. https://doi.org/10.2478/logos-2020-0004.

Boomeri, M., Naruyi, S. & Ghodsi, M.R. (2020). Petrography and geochemistry of igneous rocks and Pb mineralization in Chasorbi area, south of Zahedan, southeastern Iran. Scientific Quarterly Journal of Geosciences, 29 (116), 3-14. https://sid.ir/paper/402528/en.

Camp, V. & Griffis, R. (1982). Character, genesis and tectonic setting of igneous rocks in the Sistan suture zone, eastern Iran. Lithos, 15(3), 221-239. https://doi.org/10.1016/0024-4937(82)90014-7.

Christoph, B., Karsten, M.H., Philipp, A.B. & Stefan, H.K. (2017). Primitive andesites from the Taupo Volcanic Zone formed by magma mixing. Contributions to Mineralogy and Petrology, 172 (5), 33-47. https://ui.adsabs.harvard.edu/link_gateway/2017CoMP..172...33B/doi:10.1007/s00410-017-1354-0.

Condie, K.C. (1999). Mafic crustal xenoliths and the origin of the lower continental crust. Lithos, 46(1), 95-101. https://doi.org/10.1016/S0024-4937(98)00056-5.

Delavari, M., Mehrabi, B., Zelenski, M., Chaplygin, I., Nekrylov, N., Shakeri, A., & Taran, Y. (2022). The Bazman and Taftan volcanoes of southern Iran: Implications for along-arc geochemical variation and magma storage conditions above the Makran low-angle subduction zone. Journal of Asian Earth Sciences, 233, 105259. https://doi.org/10.1016/j.jseaes.2022.105259.

Eftekharnezhad, J. (1992). Geological map of Dorjine, 1:100000, Geological Survey of Iran, Tehran.

Faisala, M., Yanga, X., Khalifa, I.H., Amudaa, A.K. & Sun, Ch. (2020). Geochronology and geochemistry of Neoproterozoic Hamamid metavolcanics hosting largest volcanogenic massive sulfide deposits in Eastern Desert of Egypt: Implications for petrogenesis and tectonic evolution. Precambrian Research, 344, 105751. https://doi.org/10.1016/j.precamres.2020.105751.

Farhoudi, G. & Karig, D.E. (1977). Makran of Iran and Pakistan as an active arc system. Geology, 5(11), 664-668. https://ui.adsabs.harvard.edu/link_gateway/1977Geo.....5..664F/doi:10.1130/0091-7613(1977)5%3C664:MOIAPA%3E2.0.CO;2.

Floyd, P., Kelling, G., Gökçen, S. & Gökçen, N. (1991). Geochemistry and tectonic environment of basaltic rocks from the Misis ophiolitic mélange, south Turkey. Chemical Geology, 89, 263-280. https://doi.org/10.1016/0009-2541(91)90020-R.

Ghasemi, H., Sadeghian, M., Kord, M. & Khanalizadeh, A. (2010). The evolution mechanisms of Zahedan granitoidic batholith, southeast Iran. Iranian Society of Crystallography and Mineralogy, 17(4), 551-578. https://www.academia.edu/108254355.

Gunnlaugsson, H.P., Helgason, O., Kristj´ansson, L., Nørnberg, P., Rasmussen, H., Steinþ´orsson, S. & Weyer, G. (2006). Magnetic properties of olivine basalt: Application to Mars. Physics of The Earth and Planetary Interiors, 154(3-4), 276-289. http://dx.doi.org/10.1016/j.pepi.2005.09.012.

Gust, D.A. & Perfit, M.R. (1987). Phase relations of a High-Mg basalt from the Aleutian island arc: implications for primary island arc basalts and High-Al basalts. Contributions to Mineralogy and Petrology, 97, 7-18. https://doi.org/10.1007/BF00375210.

Hall, A. (1996). Igneous petrology. Longman, New York, 551pp.

Harangi, S., Downes, H., Thirlwall, M. & Gmeling, K. (2007). Geochemistry, Petrogenesis and Geodynamic Relationships of Miocene Calc-alkalineVolcanic Rocks in the Western Carpathian arc, Eastern Central Europe. Journal of petrology, 48(12), 2261-2287. https://doi.org/10.1093/petrology/egm059.

Haschke, M., Siebel, W., Günther, A. & Scheuber, E. (2002). Repeated crustal thickening and recycling during the Andean orogeny in north Chile (21–26 S). Journal of Geophysical Research: Solid Earth, 107(B1), ECV 6-1-ECV 6-18. https://doi.org/10.1029/2001JB000328.

Hastie, A.R., Keer, A.C., Pearce, J.A. & Mitchell, S.F. (2007). Classification of altered volcanic island arc rocks using immobile trace elements: development of the Th-Co discrimination. Journal of Petrology, 48(12), 2341-2357. https://doi.org/10.1093/petrology/egm062.

Hoang, N., Itoh, J. & Miyagi, I. (2011). Subduction components in Pleistocene to recent Kurile arc magmas in NE Hokkaido, Japan. Journal of Volcanology and Geothermal Research, 200(3-4), 255-266. https://doi.org/10.1016/j.jvolgeores.2011.01.002.

Hollister, L.S. & Gancarz, A.J. (1971). Compositional sector-zoning in clinopyroxene from the Narce area, Italy. American Mineralogist: Journal of Earth and Planetary Materials, 56, 959-979.

Keshtgar, S., Boomeri, M., Kananian, A. & Nazari, M. (2017). Geochemistry and tectonic setting of Zargoli granodiorite in Sistan suture zone (South East Iran). Iranian Journal of Geology, 11(42), 97-109. https://rimag.ir/en/Article/9488.

Le Bas, M.J., Le Maitre, R.W., Streckeisen, A. & Zanettin, B. (1986). A Chemical classification of volcanic rocks Based on the Total- Alkali- Silica. Diagram. Journal of Petrology, 27(3), 745-750. https://doi.org/10.1093/petrology/27.3.745.

Le Maitre, R.W. (1989). A Classification of Igneous Rocks and Glossary of Terms. Blackwell. Oxford, 193 pp.

Li, P., Yu, X., Li, H., Qiu, J. & Zhou, X. (2013). Jurassic-Cretaceous tectonic evolution of Southeast China: geochronological and geochemical constraints of Yanshanian granitoids. International Geology Review, 55(10), 1202-1219. https://doi.org/10.1080/00206814.2013.771952.

Martin, H. (1999). Adakitic magmas: modern analogues of Archaean granitoids. Lithos, 46(3), 411-429. https://doi.org/10.1016/S0024-4937(98)00076-0.

Middlemost, E.A.K. (1975). The basalt clan. Earth Science Reviews, 11(4), 337-364. https://doi.org/10.1016/0012-8252(75)90039-2.

Mohammadi, A., Burg, J.-P. & Winkler, W. (2016). Detrital zircon and provenance analysis of Eocene-Oligocene strata in the South Sistan suture zone, southeast Iran: Implications for the tectonic setting. The Geological Society of America Bulletin, 8(6), 615-632. https://doi.org/10.1130/L538.1.

Mohammadi, A., Burg, J.-P., Winkler, W., Ruh, J. & Von Quadt, A. (2016b). Detrital zircon and provenance analysis of Late Cretaceous-Miocene on shore Iranian Makran strata: Implications for the tectonic setting. Geological Society of America Bulletin, 128 (9-10), 1481-1499. https://doi.org/10.1130/B31361.1.

Moinevaziri, H. (1985). Volcanism tertiar et quaternair en Iran. PhD Thesis, Faculty of Siences, Orsay University, France.

Niu, Y. (2021). Lithosphere thickness controls the extent of mantle melting, depth of melt extraction and basalt compositions in all tectonic settings on Earth- A review and new perspectives. Earth-Science Reviews, 217, 103614. https://doi.org/10.1016/j.earscirev.2021.103614.

Omidianfar, S., Monsef, I, Rahgoshay, M., Shafaii Moghadam, H., Cousens, B., Chen, M., Rajabpour, Sh. & Zheng, J. (2023). Neo-Tethyan subduction triggered Eocene–Oligocene magmatism in eastern Iran. Geological Magazine, 160(3), 490-510. https://doi.org/10.1017/S0016756822001066.

Özdemir, Y. (2011). Volcanostratigraphy and petrogenesis of Süphan stratovolcano. Ph.D. Thesis, Middle East Technical University, Ankara, Turkey, 279 pp. https://hdl.handle.net/11511/21137.

Pan, F.-B., Jin, C., He, X., Tao, L., & Jia, B.-J. (2021). A plate-mantle convection system in the West Pacific revealed by tertiary ultramafic-mafic volcanic rocks in Southeast China. Earth and Space Science, 8(11), e2020EA001324. https://doi.org/10.1029/2020EA001324.

Pang, K.N., Chung, S.L., Zarrinkoub, M.H., Chiu, H.Y. & Hua, X. (2014). On the magmatic record of the Makran arc, southeastern Iran: Insights from zircon U-Pb geochronology and bulk-rock geochemistry. Geochemistry, Geophysics, Geosystems, 15, 2151-2169. https://ui.adsabs.harvard.edu/link_gateway/2014GGG....15.2151P/doi:10.1002/2014GC005262.

Pang, K.N., Chung, S.L., Zarrinkoub, M.H., Khatib, M.M., Mohammadi, S.S., Chiu, H.Y., Chu, C.H., Lee, H.Y. & Lo, C.H. (2013). Eocene–Oligocene post-collisional magmatism in the Lut–Sistan region, eastern Iran: Magma genesis and tectonic implications. Lithos, 180-181, 234-251. https://ui.adsabs.harvard.edu/link_gateway/2013Litho.180..234P/doi:10.1016/j.lithos.2013.05.009.

Pearce, J.A. & Gale, G.H. (1977). Identification of ore-deposition environment from trace element geochemistry of associated igneous host rocks. Geological Society, London, Special Publications, 7, 14-24. https://doi.org/10.1144/GSL.SP.1977.007.01.03.

Pearce, J.A. & Norry, M.J. (1979). Petrogenetic Implications of Ti, Zr, Y, and Nb Variations in Volcanic Rocks. Contributions to Mineralogy and Petrology, 69(1), 33-47. https://doi.org/10.1007/BF00375192.

Pearce, J.A. & Peate, D.W. (1995). Tectonic implications of the composition of volcanic arc magmas. Earth and Planetary Science Letters, 23, 251-285. https://doi.org/10.1146/annurev.ea.23.050195.001343.

Pearce, J.A. & Peate, D.W. (1995). Tectonic Implications of the Composition of Volcanic Arc Magmas. Annual Review Of Earth And Planetary Sciences, 23, 251-286. https://ui.adsabs.harvard.edu/link_gateway/1995AREPS..23..251P/doi:10.1146/annurev.ea.23.050195.001343.

Pearce, J.A. (1982). Trace element characteristics of lavas from destructive plate boundaries. Orogenic andesites and related rocks, 8, 525-548. http://refhub.elsevier.com/S0301-9268(19)30564-9/h0500.

Pearce, J.A. (1983). Role of the sub-continental lithosphere in magma genesis at active continental margins. In: Hawkesworth C.J., Norry M.J., (eds.) Continental basalts and mantle xenoliths, Nantwich, Cheshire: Shiva Publications, 230-249. https://orca.cardiff.ac.uk/id/eprint/8626.

Pearce, J.A. (2008). Geochemical fingerprinting of oceanic basalts with applications to ophiolite classification and the search for Archean oceanic crust. Lithos, 100, 14-48. https://doi.org/10.1016/j.lithos.2007.06.016.

Pearce, J.A. (2014). Immobile element fingerprinting of ophiolites. Elements, 10(2), 101-108. https://doi.org/10.2113/gselements.10.2.101.

Plank, T. & Langmuir, C.H. (1998). The chemical composition of subducting sediment and its consequences for the crust and mantle. Chemical Geology, 145, 325-394. https://doi.org/10.1016/S0009-2541(97)00150-2.

Prelevic, D., Wehrheim, S., Reutter, M., Romer, R.L., Boev, B., Bozovic, M., van den Bogaard, P., Cvetkovic, V. & Schmid, S.M. (2017). The late cretaceous Klepa basalts in Macedonia (FYROM) constraints on the final stage of Tethys closure in the Balkans. Terra Nova., 29(3), 145-153. https://doi.org/10.1111/ter.12264.

Qian, X., Feng, Q., Wang, Y., Chonglakmani, C. & Monjai, D. (2016). Geochronological and geochemical constraints on the mafic rocks along the Luang Prabang zone: Carboniferous back-arc setting in northwest Laos. Lithos, 245, 60-75. https://doi.org/10.1016/j.lithos.2015.07.019.

Rahnama-Rad, J., Sahebzadeh, B. & Mirhajizadeh, A.A. (2008). Weathering and weakness of Zahedan granitoids: A 609 rock engineering point of view. Applied Geology, 4, 247-257. https://sanad.iau.ir/en/Article/1038194.

Rojhani, E., Ghaemi, F., Bagheri, S., Li, Sh., Lom, N. & Hinsbergen, D.V. (2025). Tectonic Evolution of the Abrupt Northern Termination of the Sistan Suture Zone (Eastern Iran). Tectonophysics. https://ssrn.com/abstract=4910793.

Rudnick, R.L. & Gao, S. (2014). Composition of the continental crust, Treatise on geochemistry4. In: Reference Module in Earth Systems and Environmental Sciences (Ed. Elias, S.A.) 2nd edition, 1 -51. Elsevier, Amsterdam.

Sadeghian, M. & Valizadeh, M. (2007). Mechanism of replacement Northern part of Zahedan Granitoid. Earth Sciences Quarterly, 66, 134-159.

Sadeghian, M., Bouchez, J.L., Nedelec, A., Siqueira, R. & Valizadeh, M.V. (2005). The granite pluton of Zahedan (SE Iran): a petrological and magnetic fabric study of a syntectonic sill emplaced in a transtension Setting. Journal of Asian Earth Sciences, 25, 301- 327. https://doi.org/10.1016/j.jseaes.2004.03.001.

Safonova, I.Yu., Buslov, M.M., Simonov, V.A., Izokh, A.E., Komiya, T., Kurganskaya, E.V. & Ohno, T. (2011). Geochemistry, petrogenesis and geodynamic origin of basalts from the Katun' accretionary complex of Gorny Altai (southwestern Siberia). Russian Geology and Geophysics, 52(4), 421-442. https://doi.org/10.1016/j.rgg.2011.03.005.

Salas, P., Ruprecht, P., Hernández, L. & Rabbia, O. (2021). Out-of-sequence skeletal growth causing oscillatory zoning in arc olivines. Nature Communications, 12(1), 4069. https://doi.org/10.1038/s41467-021-24275-6.

Schoneveld, L., Barnes, S.J., Makkonen, H.V., Vaillant, M.L., Paterson, D.J., Taranovic, V., Wang, K.Y. & Mao, Y.J. (2020). Zoned pyroxenes as prospectivity indicators for magmatic Ni-Cu sulfide mineralization. Frontiers in Earth Science, 8:256. https://doi.org/10.3389/feart.2020.00256.

Sengor, A.M.C. (1990). A New Model for the Late Palaeozoic-Mesozoic Tectonic Evolution of Iran and Implications for Oman, In: Robertson, A.H.F., Searle, M.P. and Ries, A.C., Eds., The Geology and Tectonics of the Oman Region, Geological Society Special Publications, 49, 797-831. http://dx.doi.org/10.1144/gsl.sp.1992.049.01.49.

Sepidbar, F. (2018). Identification of Eocene-Oligocene magmatic pulses associated with flare-up in east Iran: Timing and sources. Gondwana Research, 57, 141-156. https://profdoc.um.ac.ir/paper-abstract-1099044.html

Shervais, J.W. (1982). Ti-V Plots and the Petrogenesis of Modern and Ophiolitic Lavas. Earth and Planetary Science Letters, 59(1), 101-118. https://doi.org/10.1016/0012-821X(82)90120-0.

Smith, E.I., Sánchez, A., Walker, J.D. & Wang, K. (1999). Geochemistry of mafic magmas in the Hurricane Volcanic field, Utah: implications for small - and large -scale chemical variability of the lithospheric mantle. Journal of Geology, 107, 433-448. https://doi.org/10.1086/314355.

Sun, S.S. & McDonough, W.F. (1989). Chemical and isotopic systematics of oceanic basalts: implications for mantle composition and processes. Geological Society, London, Special Publications 42, 313-345. http://refhub.elsevier.com/S0301-9268(19)30564-9/h0680.

Tirrul, R., Bell, I., Griffis, R. & Camp, V. (1983). The Sistan suture zone of eastern Iran. Geological Society of America Bulletin, 94(1), 134-150. https://doi.org/10.1130/0016-7606(1983)94<134:TSSZOE>2.0.CO;2.

Walker, R. & Jackson, J. (2004). Active tectonics and late Cenozoic strain distribution in central and eastern Iran. Tectonics, 23(5), TC5010. http://dx.doi.org/10.1029/2003TC001529.

Wood, D.A. (1980). The application of a Th-Hf-Ta diagram to problems of tectonomagmatic classification and to establishing the nature of crustal contamination of basaltic lavas of the British Tertiary Volcanic Province. Earth and Planetary Science Letters, 50(1), 11-30. https://doi.org/10.1016/0012-821X(80)90116-8.

Woodhead, J., Eggins, S. & Gamble, J. (1993). High field strength and transition element systematics in island arc and back-arc basin basalts: evidence for multi-phase melt extraction and a depleted mantle wedge. Earth and Planetary Science Letters, 114(4), 491–504. https://doi.org/10.1016/0012-821X(93)90078-N.

Yoder, H.S. & Tilley, C.E. (1962). Origin of basalt magmas: an experimental study of natural and synthetic rock systems. Journal of Petrology, 3(3), 342-532. https://doi.org/10.1093/petrology/3.3.342.

Zeng, G., Chen, L-H., Xu, X-Sh., Jiang, Sh-Y. & Hofmann, A.W. (2010). Carbonated mantle sources for Cenozoic intra-plate alkaline basalts in Shandong, North China. Chemical Geology, 273(1-2), 35-45. http://dx.doi.org/10.1016/j.chemgeo.2010.02.009.

Zhang, T.Y., Deng, J., Wang, M., Li, C., Zhang, L. & Sun, W. (2022). Geochemistry and genesis of the Nadun Nb-enriched arc basalt in the Duolong mineral district, western Tibet: Indication of ridge subduction. Geoscience Frontier, 13, 101283. https://doi.org/10.1016/j.gsf.2021.101283.

Zhou, X.M., Sun, T., Shen, W.Z., Shu, L.S. & Niu, Y.L. (2006). Petrogenesis of Mesozoic granitoids and volcanic rocks in South China: a response to tectonic evolution. Episodes 29(1), 26-33. https://doi.org/10.18814/epiiugs/2006/v29i1/004.